Title
THE PHYSICS OF HEAVY-ION RADIOGRAPHY AND HEAVY-ION COMPUTERIZED TOMOGRAPHY

Author
Holley, W.R.

Publication Date
1982-03-01

LBL-14316

Lawrence Berkeley Laboratory
UNIVERSITY OF CALIFORNIA

Presented at the International Workshop on Physics and Engineering in Medical Imaging, Pacific Grove, CA, March 15-18, 1982

THE PHYSICS OF HEAVY-ION RADIOGRAPHY AND HEAVY-ION COMPUTERIZED TOMOGRAPHY

W.R. Holley, J.I. Fabrikant, C.A. Tobias, and E.V. Benton

March 1982

Donner

Biology & Medicine Division

Prepared for the U.S. Department of Energy under Contract DE-AC03-76SF00098

DISCLAIMER

LBL-14316

THE PHYSICS OF HEAVY-ION RADIOGRAPHY AND HEAVY-ION COMPUTERIZED TOMOGRAPHY [1,2]

W. R. Holley, J. I. Fabrikant and C. A. Tobias
Division of Biology and Medicine
Lawrence Berkeley Laboratory
University of California
Berkeley, California

and

E. V. Benton
Department of Physics
University of San Francisco
San Francisco, California

[1] Presented at the International Workshop on Physics & Engineering in Medical Imaging, Pacific Grove, California, March 15-18, 1982.

[2] Research supported by the Office of Health and Environmental Research of the U.S. Department of Energy under contract DE-AC03-76SF00098.

THE PHYSICS OF HEAVY-ION RADIOGRAPHY AND HEAVY-ION COMPUTERIZED TOMOGRAPHY

William R. Holley, Jacob I. Fabrikant, and Cornelius A. Tobias
Lawrence Berkeley Laboratory, University of California, Berkeley, CA

and Eugene V. Benton
University of San Francisco, San Francisco, CA

Abstract

Techniques are being developed at Lawrence Berkeley Laboratory for heavy-ion projection radiography and heavy-ion computerized tomography using high-energy carbon, oxygen and neon beams. The physical characteristics of heavy-ion beams, such as range straggling and multiple coulomb scattering, affecting image spatial and density resolution and radiation dose are discussed. The methods of beam production and exposure, particle detection, digitization of data, and computer analysis and reconstruction of heavy-ion images are described. Comparisons between heavy-ion CT images and x-ray CT images of phantoms and tissue specimens are made, and the physical bases for differences of the two modalities are discussed.

Introduction

At Lawrence Berkeley Laboratory, radiographic and computerized tomographic studies of phantom and tissue specimens using a variety of energetic heavy particles have shown promise for imaging details of soft tissue structures[1-8]. The source of accelerated heavy ions is the Bevalac[9,10], an accelerator complex completed in 1975 (Figure 1). Using the HILAC (Heavy-Ion Linear Accelerator) as an injector, the Bevalac can accelerate fully stripped atomic nuclei from carbon (atomic number Z=6) to krypton (Z=34). Useful ranges in tissue of 40 cm or more are available. Radiographic studies to date have been conducted with helium, carbon, oxygen, and neon beams.

Fundamental Principles of Heavy-Ion Radiography

Figure 2 illustrates the technique used at Lawrence Berkeley Laboratory for heavy-ion radiography. A nearly parallel stream of heavy particles crosses the object to be radiographed and stops in a stack of plastic foils. The foils are nuclear track detectors, originally developed to study heavy primary cosmic rays and to record tracks due to nuclear fission fragments. The stopping point distribution in the plastic detector stack corresponds to the residual range distribution of the particles after crossing the object.

The plastic foils used for heavy-ion imaging are insensitive to the passage of low-LET particles; high-LET particles cause a lesion in the plastic that can be developed by the application of concentrated sodium hydroxide until a tiny conical impression or hole forms. The plastics that we are using, Lexan and cellulose nitrate, are only sensitive to stopping heavy particles; it is practical to use them for particles with atomic numbers 6 through 10. The information on each pastic sheet is transferred by an optical scanning method to a computer for further quantitation and eventual display.

Compared to diagnostic x-rays, heavy ions (e.g. carbon) are much more sensitive to small electron density differences (density resolution) in the subject, which can be visualized with higher contrast and significantly lower doses. On the other hand, the lateral (spatial) resolution of x-rays (i.e., in planes perpendicular to the direction of the beam) is better than that of heavy particles.

The transverse spatial information in the heavy-ion image is in principle limited by the fact that the heavy ions do not quite travel in straight lines but undergo small angle scatterings with target nuclei. The effects of multiple coulomb scattering are such as to smear out transversly an incident pencil line of beam into an approximately Gaussian distribution with a standard deviation which varies approximately linearly with range and inversly with approximately the 0.6 power of the incident particle mass.

An approximate expression for the standard deviation is given by the following empirical formula valid for incident particles of mass number A, charge Z, and range R in water:

$$\sigma_{mcs}(\mathrm{cm}) \simeq \frac{0.0294\ R^{0.896}}{Z^{0.207}\ A^{0.396}}$$

Figure 3B shows the dependence of the lateral scattering on object thickness for a feature on the upstream edge of the object. The integrated density or depth resolution (the resolution for measuring the stopping power of an object) is limited by energy spread of the beam (small for Bevatron beams) and by statistical fluctuations in the energy loss process. The variation in the stopping points of a monoenergetic beam, that is, range straggling, also follows an approximately Gaussian distribution with a standard deviation nearly proportional to the range and to the inverse square root of the particle mass. Figure 3A shows these relationships for several typical beam particles as functions of range in water.

The standard deviation for range straggling for particles of mass number A and range R (in cm) of tissue- or water-equivalent material is given by the following approximate expression:

$$\sigma_{RS}(\mathrm{cm}) \approx \frac{0.012\ R^{0.951}}{\sqrt{A}}$$

This formula represents the standard deviation of the stopping distribution of beam particles. The mean stopping point of a set of N stopping particles in a transverse pixel of interest has an error given by the SD of the distribution divided by the square root of the number of particles so that the density accuracy is proportional to $1/\sqrt{N}$ or equivalently $1/\sqrt{\text{dose}}$.

Computer Processing and Data Analysis

Although individual nuclear detector stack layers can be viewed qualitatively as radiographs, for quantitative analysis it is necessary to obtain a computer synthesis of the digitized information from all of the individual layers. The physical aspects of the digitization and synthesis process are illustrated in Figure 4. The individual detector layers are darkfield illuminated and scanned by a Vidicon. The signal from the Vidicon is then digitized by a high-speed analog-to-digital converter, i.e., a digitizer.

At every lateral point (pixel location) the necessary information contained in the data is the average penetration of the beam into the stack, i.e. the average stopping point of the particle R. A number of different computational approaches have been used in the determination of R. The determination is not perfectly straightforward because of the background signal contributed by the etched layers. Figure 5 shows a typical digitized signal at one particular pixel location as a function of sheet number or depth of penetration into the stack. The average stopping point for this pixel is found from a locally-truncated intensity-weighted average of the sheet numbers.

In order to obtain the best signal-to-background-noise ratio when digitizing, it is necessary both to illuminate and view the plastic sheets obliquely. To eliminate the "forshortening" distortion produced by this tilt angle (usually 45 degrees) and also other sources of distortion and nonlinearities present in the optics and electronics of the Vidicon tube and digitizer, the following procedure is used. (1) The initial set of digitized, "raw," data (typically 256 x 256 pixels for each of up to 200 sheets in a radiography stack) is reduced down to a single array of numbers representing the average stopping point R at each pixel location. (2) To remove the distortions, a grid (typically 20 x 20) of very accurately spaced points is placed in exactly the same position as the sheets and digitized. The digitizer produces an image (Figure 6) of the grid with the same distortions that are present in the digitized sheets. (3) A simple pattern recognition procedure is then used to find the position of the center of each grid point in digitized (distorted) space. The corrected image space is related to the true grid space by a simple translation and scale change. This transformation is used to relate each pixel location ic, jc in corrected space to a position XG, YG in grid space. The locations of the four nearest neighbor grid points in original distorted space as determined previously are used by means of bilinear interpolation to determine the corresponding coordinates xd, yd in distorted space. (4) Finally, to obtain the value R to associate with the position ic, jc in corrected space (i.e., position equivalent to xd, yd) bilinear interpolation between the four nearest neighbor pixels to xd, yd is used.

This procedure removes distortions from the image and in the case of single view plane radiographs result in a satisfactory final image. In general, for heavy-ion computerized tomography, however, rotations, scale changes and coordinate shifts are needed. Figure 7 illustrates a corrected image of the grid shown in Figure 6, with the distortions removed.

Heavy-Ion Computerized Tomography

Because of the quantitative character of the heavy particle radiographs, computerized tomography is a logical extension of the heavy particle radiography technique. This extension is accomplished by converting one spatial coordinate into the projection angle coordinate. The beam is confined by a horizontal slit collimator. After passing through the collimator, the beam passes through the object to be imaged, which is immersed in a water bath. For CT scanning, the object is rotated about a vertical axis, 1 to 3 degrees between successive exposures. A narrow horizontal strip of exposure is then produced in the detector stack by a final collimator which is placed immediately downstream from the immersion bath and upstream from the stack. Between beam pulses, while the radiographed object is rotated, the stack is translated either upward or downward in increments equal to the width of the final collimator.

The projection value required for input into the tomographic reconstruction algorithm is the difference in the range of beam passing through the radiographed object and through a reference material (usually chosen to be water)[5]. For this purpose the projections include a strip on each side of the object where the beam only passes through water. In addition, when possible, a full projection is made with the radiographed object replaced by water so that a true R(object)-R(water) difference can be formed. Possible variations in beam energy from pulse to pulse (i.e., projection to projection) are corrected at the same time by adjusting the water correction projection to match the water strips at the edges of each projection before making the subtraction.

Finally, the corrected projection data that have remained in the form of an N x N array (usually 256 x 256) are converted to an array with one row (or record) for each projection. Most of the heavy-ion tomographic exposures have been taken with angular steps of about 2 degrees and therefore require about 90 projections. At this point in the analysis any extra projections taken to ensure against loss of data at the beginning or end of the rotations are eliminated and the data properly normalized for input into the reconstruction programs. Bilinear interpolation is used to reduce the array from 256 x 256 to 90 x 256, which is the array most frequently used.

Reconstruction and Display

For heavy-ion CT reconstruction a filtered back projection algorithm is applied, using a modified Shepp-Logan[11,12] method from the Budinger-Huesman Donner reconstruction program package[13]. The results of the computations are distributions of electronic stopping powers, usually in terms of the heavy-ion number, τ, defined by the following equation:

$$\tau = 1000(\sigma_t/\sigma_w - 1) \approx 1000(n_t/n_w - 1)$$

where σ_t and σ_w are linear stopping power values and n_t and n_w are the electron densities of the target material and water, respectively. This information is not the same as that displayed in x-ray CT scans; for x-ray CT,

$$H = 1000(\mu_t/\mu_w - 1)$$

where μ_t and μ_w are the average or "effective" linear x-ray attentuation coefficients of target and water, respectively. Comparison of x-ray and of heavy-ion CT scans gives significant information on the electronic composition of the medium scanned.

Computerized Tomography of Phantoms

In order to optimize the procedure of mathematical CT reconstruction of heavy-ion data, some simple phantoms were constructed; their use allowed a study of the efficacy of the procedures at each step. By this method several artifacts related to heavy-ion tomography have been found, and as these have been reduced, the computerized tomographs showed considerable improvement.

One phantom consisted of a column of water with cylindrical walls. Four polystyrene test tubes were immersed into the water, each containing glucose/water test solutions. The test tubes had a diameter of 1.0 cm and wall thickness of 0.07 cm. The density of the test tube wall was 1.04. In the center of the column, a nylon rod marked the axis of rotation for the phantom. Figure 8 top shows a sinogram of this test-tube assembly, after tomographic exposures of a 0.2 cm section to a 557 MeV/amu neon beam, development, digitizing and application of special data correction programs. The image of the 90 angular projections shows correctly that the image of each test tube follows a sinusoidal curve. The walls of the test tubes are clearly resolved; the image is slightly blurred due to multiple scattering. The vertical stripe at the center is due to the nylon rod; the straightness of this image indicates that it was very near the center of the rotation. Figure 8 bottom shows a sinogram of the same assembly, before the correction program. Horizontal stripes indicate individual scans at each angle. The right side is darker than the left, because the water bath container was thicker on one side than the other (i.e., wedge shaped). The horizontal striped appearance is due to a slightly different neon particle energy in consecutive pulses from the Bevalac. The range deviations were of the order of 0.5 percent. These two artifacts were corrected by adjusting the range value proportionately in each pixel for uniform range in water.

Figure 9 shows a reconstruction of the test tube pattern with neon ions. This image may be compared to an x-ray CT reconstruction, Figure 10, obtained of the same phantom with a General Electric 7800 CT scanner at the Department of Radiology, University of California, San Francisco. Both computerized tomograms reproduce the pattern, but with notable differences. The walls of the test tubes appear whiter than background in the neon radiograph and darker than background in the x-ray CT scan. This is because the electron density of the wall, n_{et}, is greater than that of water, n_{ew}, so that $\tau > 0$. The x-ray absorption coefficient of the wall is less than that of water, $H < 0$. The difference may be due to the fact that the carbon in polystyrene absorbs x-rays less efficiently than the oxygen in water.

The test tubes were filled with glucose dissolved in water at different concentrations. Table I compares these values with the measurements obtained in the two scans. Thus, the neon-ion (557 MeV/amu) radiograph correctly predicted the densities in each tube. In the x-ray CT scan, there was much more noise and variation in the background. These tests have demonstrated that heavy-ion computerized tomography can resolve structures as small as 0.07 cm, and density differences of 0.005.

Table 1. Comparison of Glucose Concentrations in Test Tube Phantom

Test Tube		Actual Density	τ Neon	H 80 kVp
Inside	No. 1	1.0 (water)	0±0.5	6±1
	No. 2	1.005	5±0.6	7±0.8
	No. 3	1.01	9±0.5	13±1
	No. 4	1.015	17±0.7	22±1.6
Outside Background		1.0 (water	0±0.6	4-21±4

Imaging Tissue Specimens

The heavy-ion CT imaging method has been applied to human tissue specimens using either neon- or carbon-ion beams[14,15]. In one typical study a coronal plane of a whole human brain specimen was scanned with an 0.2 cm slit, 90 projection angles and using a 557 MeV/amu (15 cm range) beam. The heavy-ion CT reconstruction of this brain specimen (Figure 11) demonstrates high resolution of the soft tissue structures of the brain. The density resolution appears better than in the x-ray CT scan

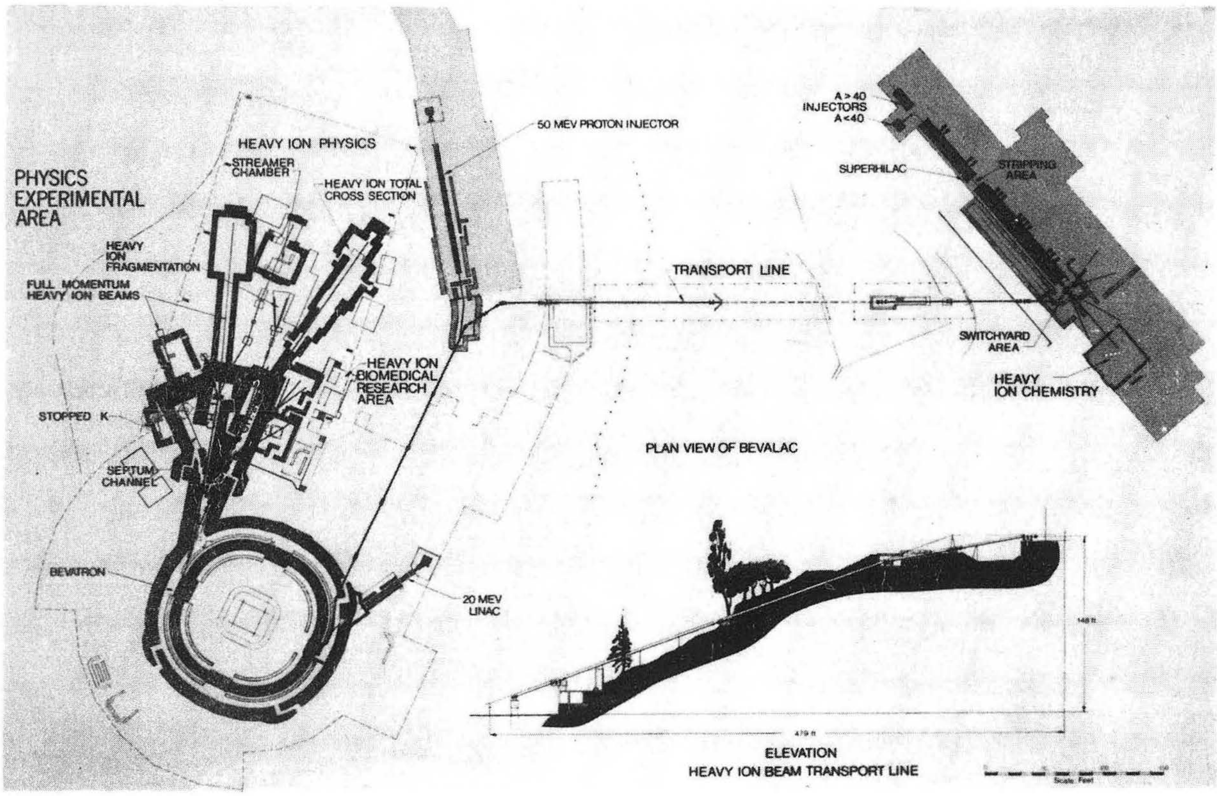

CBB740-7911

Figure 1

Diagram of the Bevalac Heavy Ion Accelerator complex at Lawrence Berkeley Laboratory showing the Superhilac injector, transfer line, Bevatron and biomedical research area.

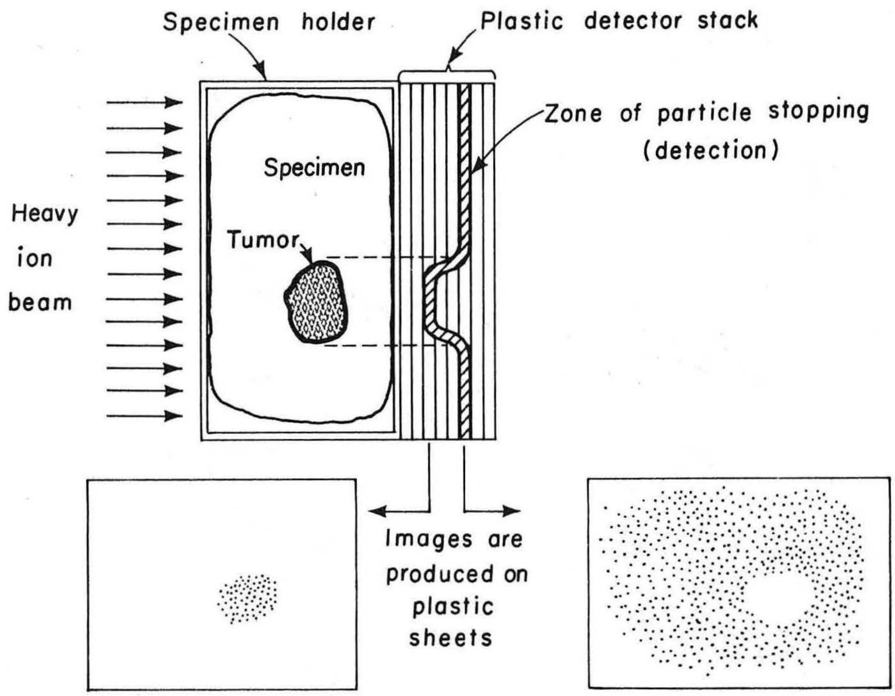

Figure 2

Principle of heavy-ion radiography with plastic nuclear track detectors. After the beam passes through the object, the heavy ions are recorded at their stopping points in the detector sheets. The patterns of etched tracks on the developed sheets constitute the radiographic images.

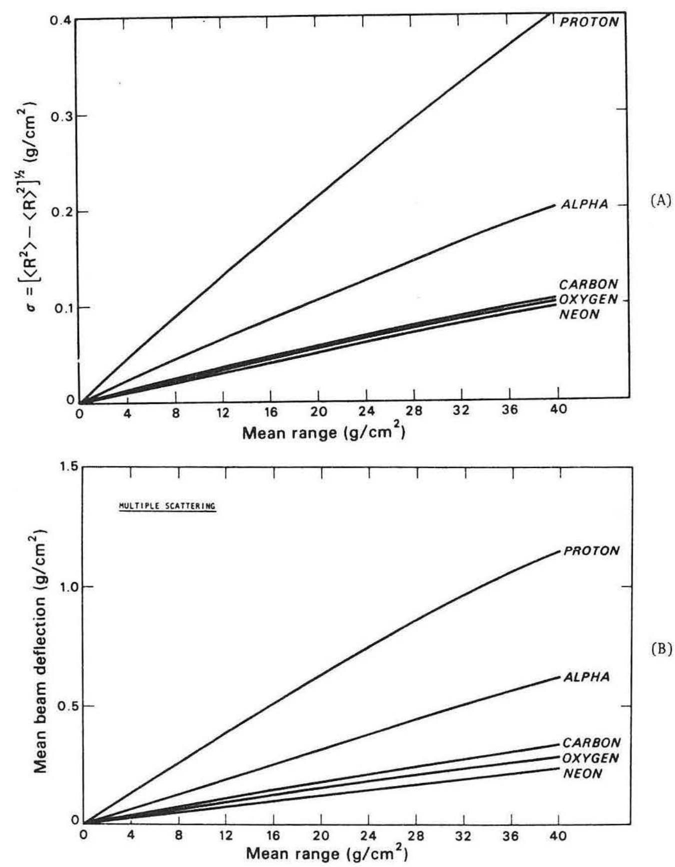

Figure 3

Heavy ions have greater depth-resolution sensitivity and contrast than protons, alpha particles or x-rays. This is shown quantitatively here where the range straggling (A) and beam deflection (B) due to multiple small-angle scattering are drawn for protons and heavier particles as functions of the range penetration in water. In (B) the imaged feature is on the upstream side of the water.

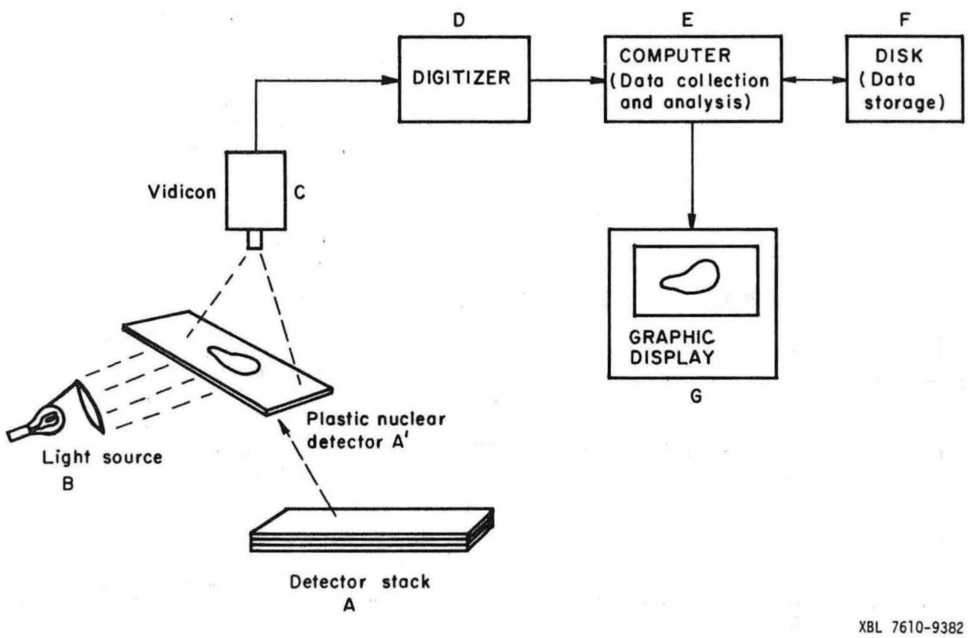

Figure 4

Diagram of computerized data analysis showing method of digitizing, using a TV vidicon, by viewing each nuclear track detector sheet in oblique light.

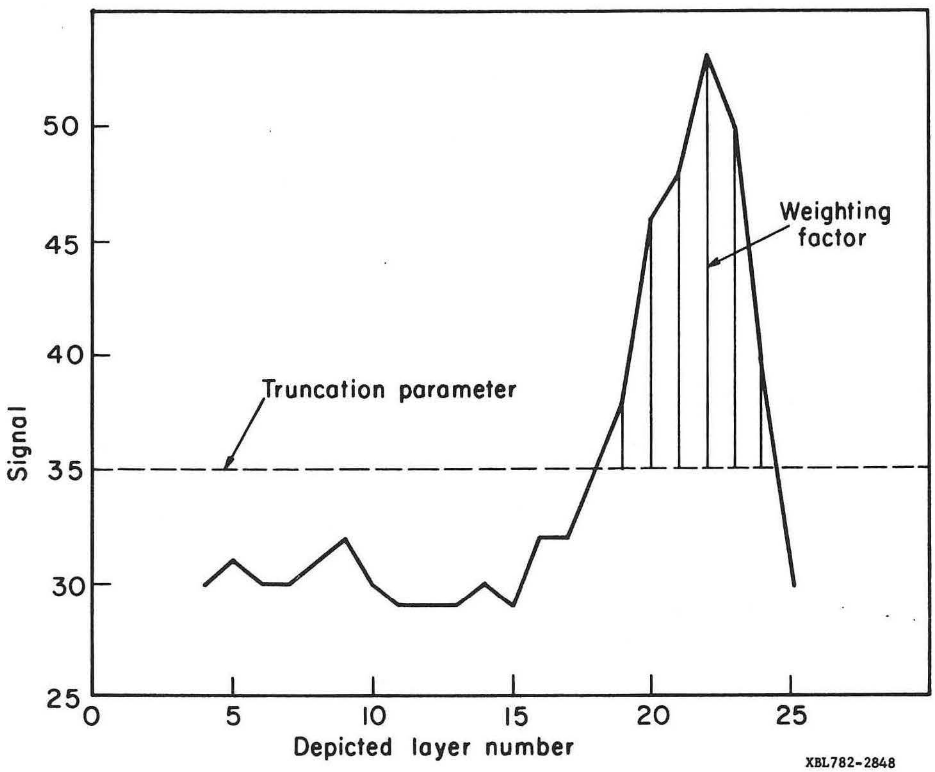

Figure 5

Typical signal intensity profile plotted versus sheet layer number. The signal due to the etched tracks is superimposed on the background signal of the etched detector layers. The area above the truncation parameter is the portion of the measured curve used in determining the average particle stopping point, R.

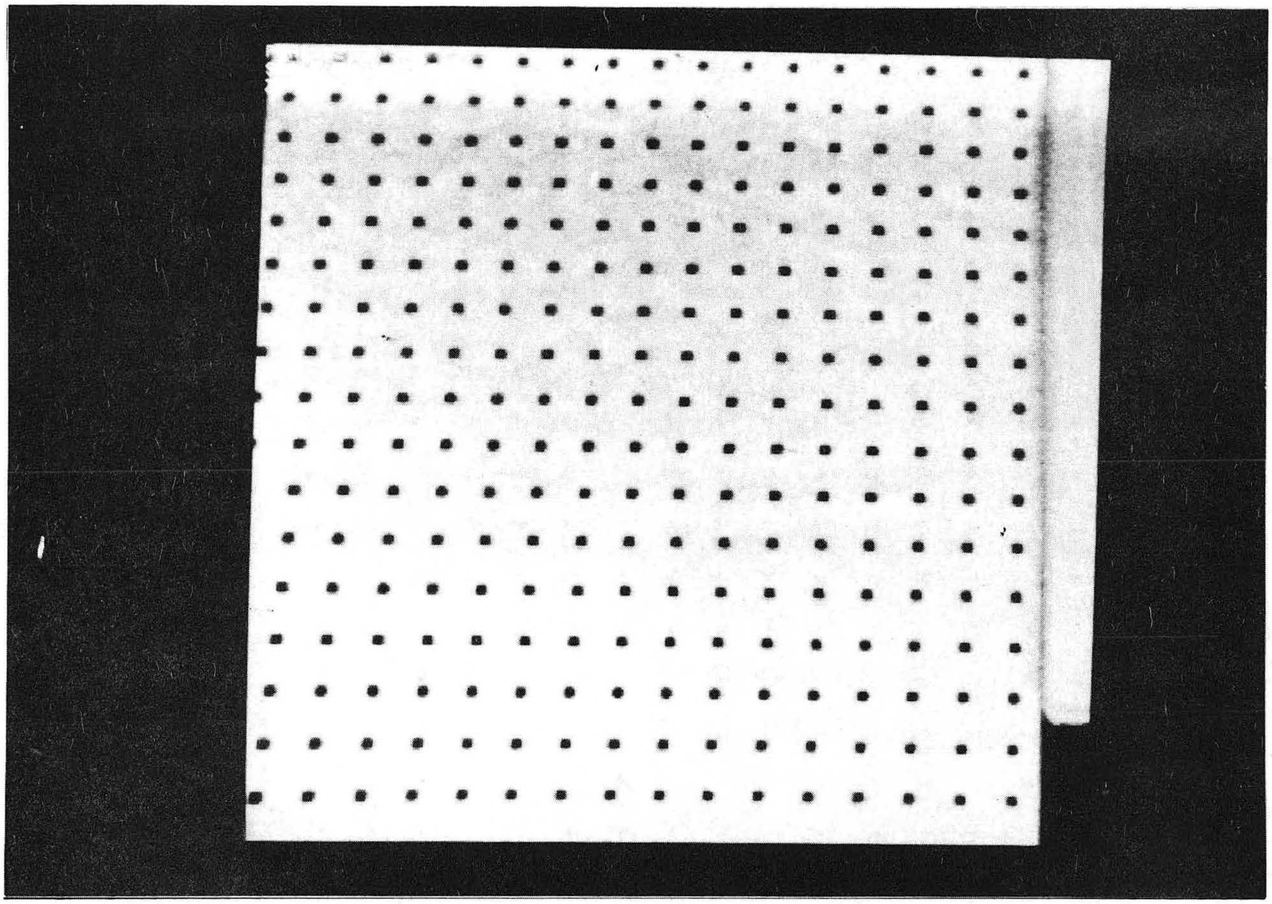

XBB809-10874

Figure 6

Digitized image of correction grid with same optical and electronic distortions present as in digitized radiographic sheets.

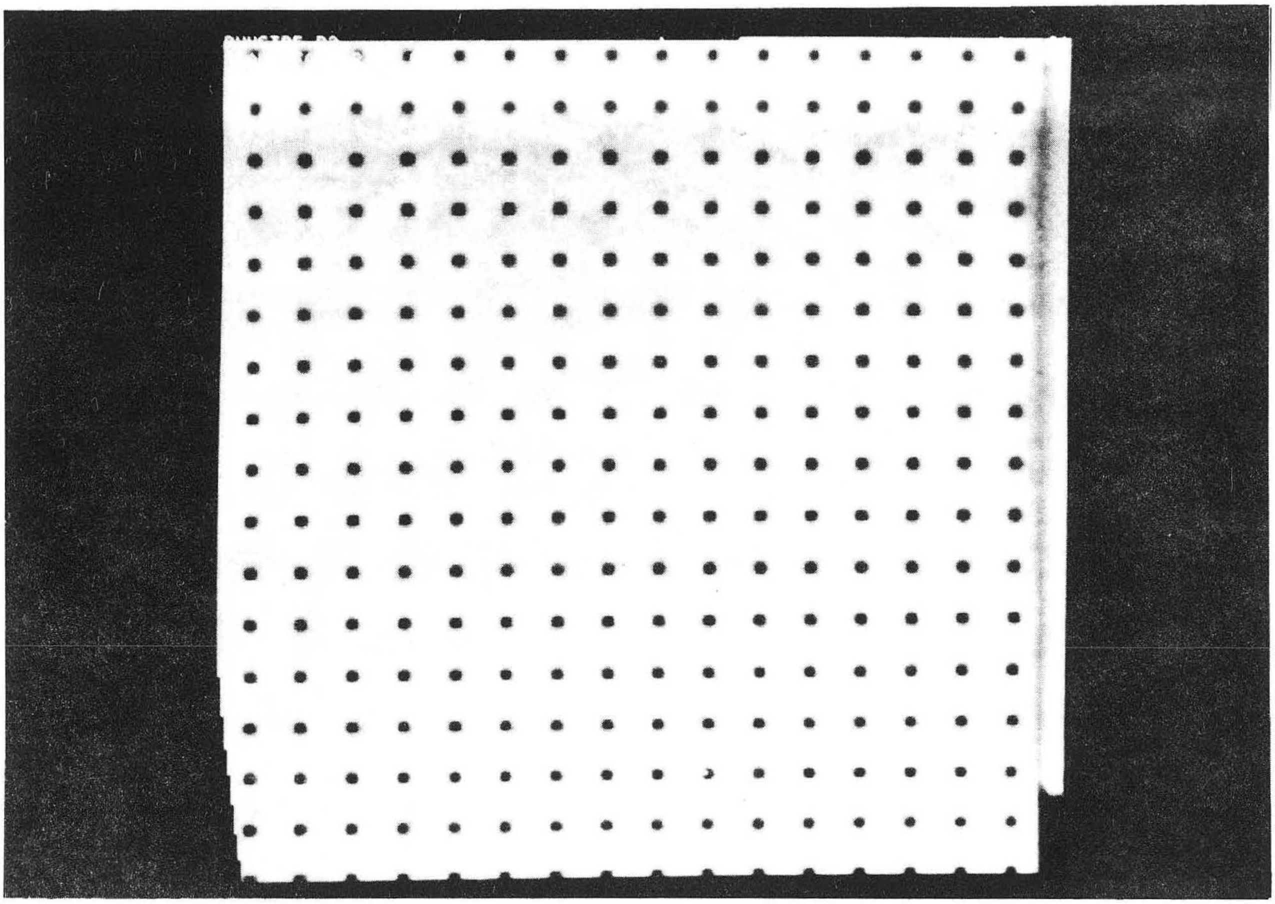

XBB809-10873

Figure 7

Corrected grid image after distortions are removed.

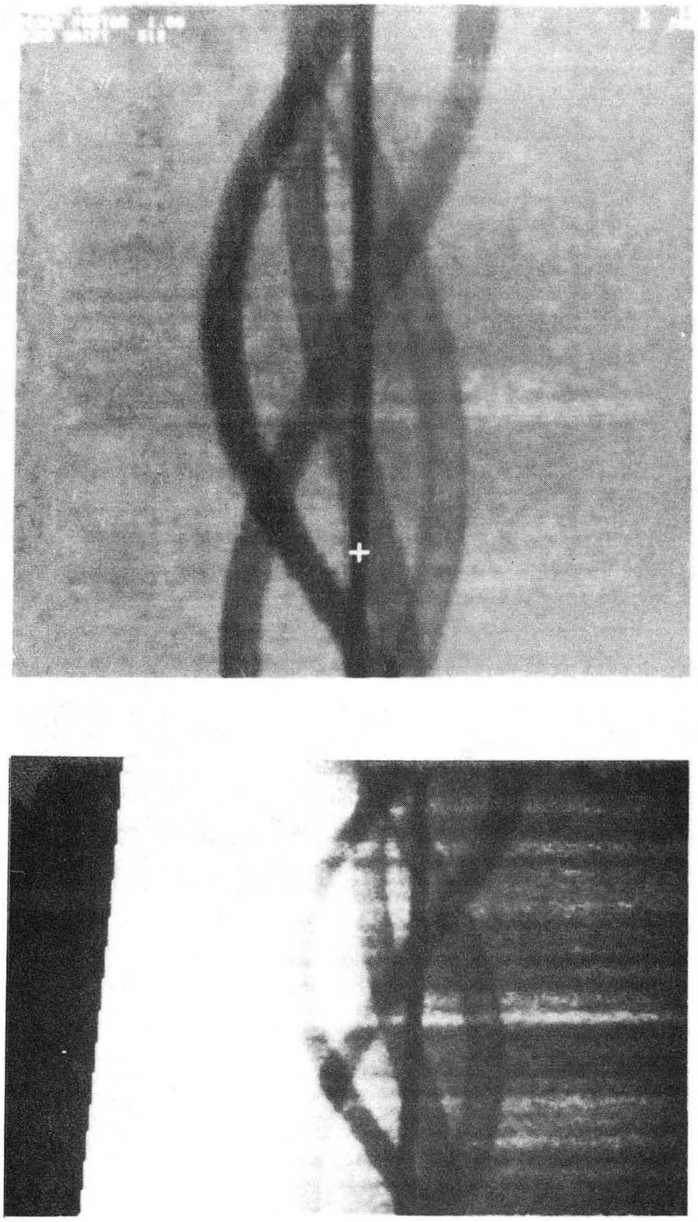

XBB809-10875A

Figure 8

Corrected (top) and uncorrected (bottom) sinograms of test-tube phantom assembly made with a 557 MeV/amu neon beam. The phantom consists of four polystyrene test-tubes, each containing test solutions of different density. The test-tube diameter is 1.0 cm; the wall thickness, 0.07 cm, and the density of the test-tube wall is 1.04. The vertical stripe in the center is a nylon rod.

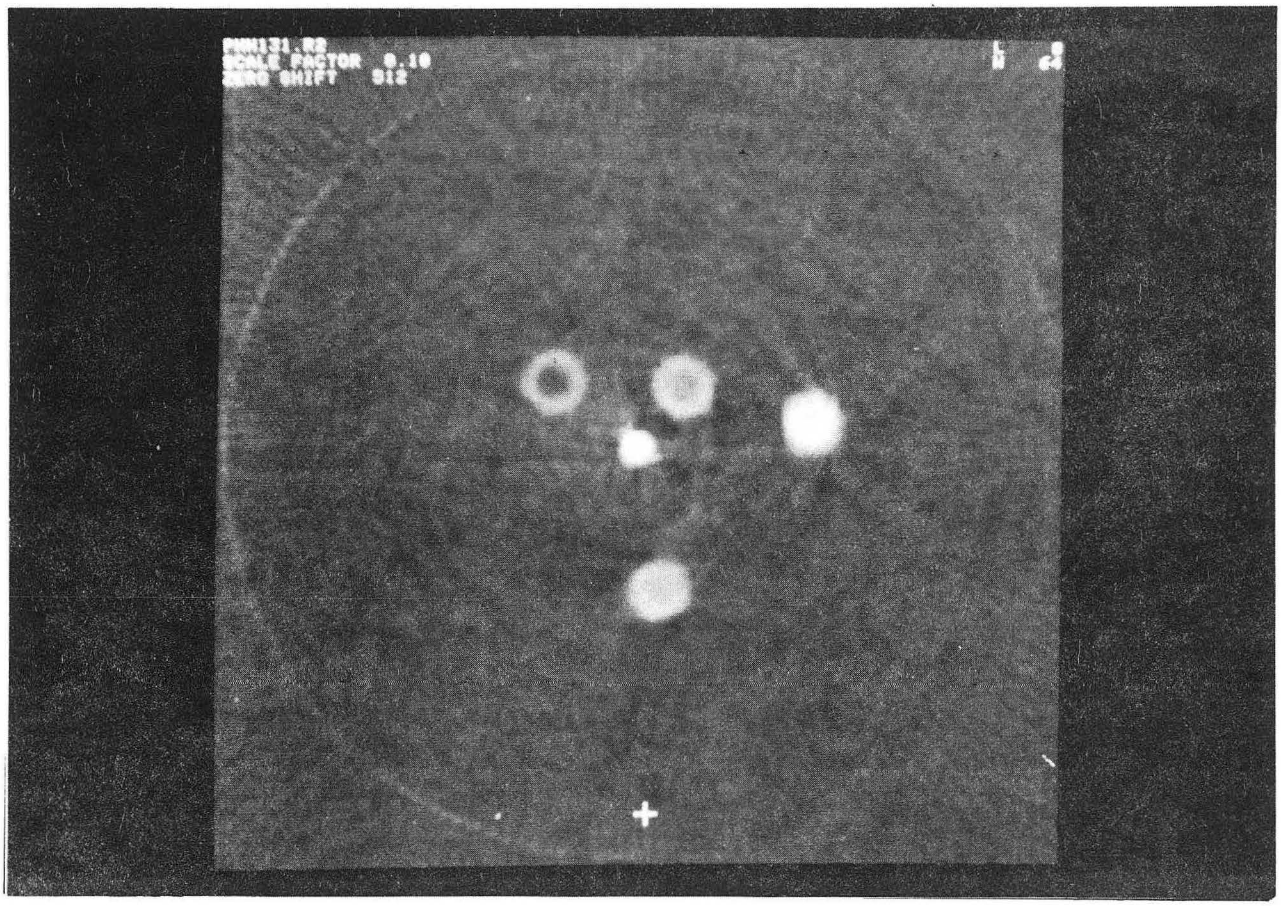

XBB809-10844

Figure 9

Neon-ion beam CT image of test-tube assembly immersed in water. The test-tube walls are white because their electronic stopping power (μ_e) is greater than that of water.

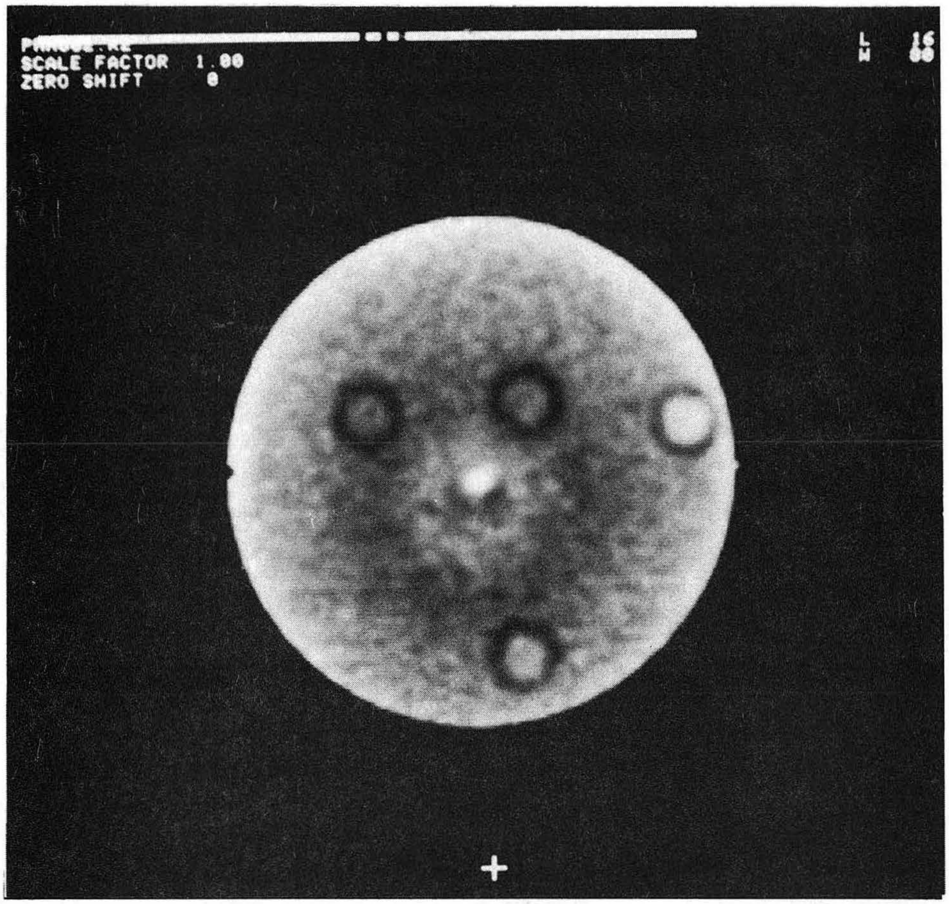

XBB809-10768

Figure 10

X-ray CT image of the assembly described above. The x-ray water background varies more than the neon-ion background. The test-tube walls appear dark because the x-ray absorption coefficient of polystyrene is smaller than that of water.

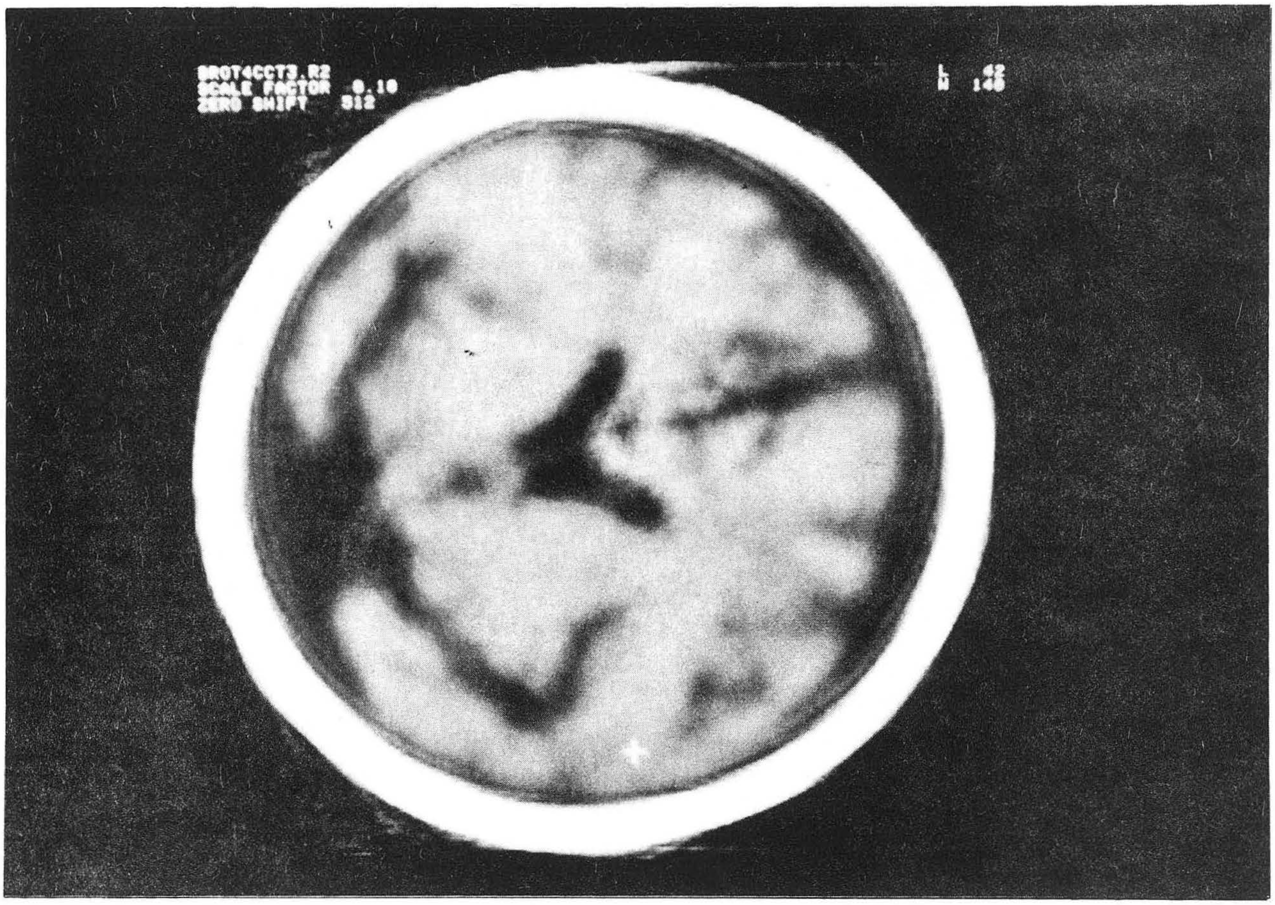

XBB809-10849

Figure 11

557 MeV/amu neon-ion CT reconstruction of human brain autopsy specimen.

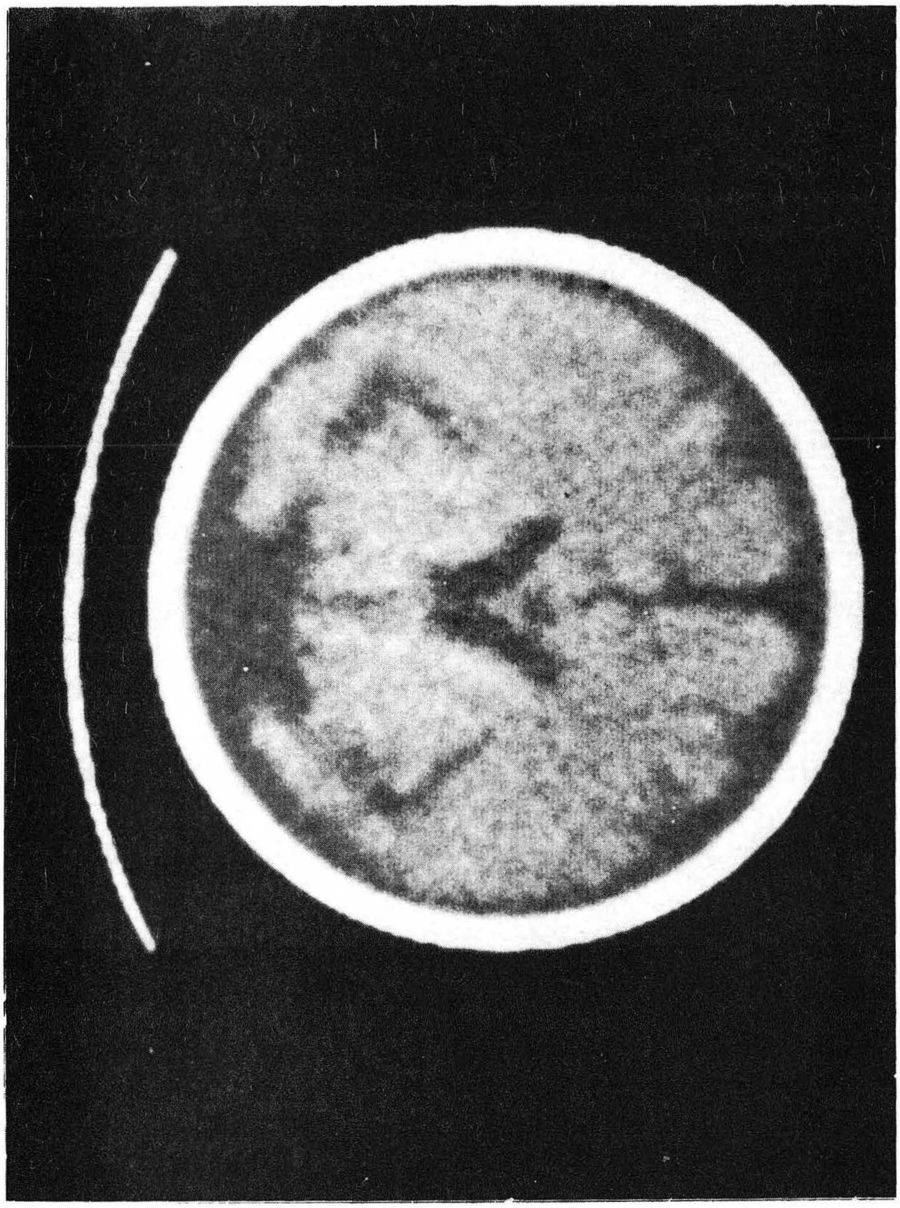

XBB809-10951

Figure 12

X-ray CT scan of human brain specimen illustrated in Figure 11.

TECHNICAL INFORMATION DEPARTMENT
LAWRENCE BERKELEY LABORATORY
UNIVERSITY OF CALIFORNIA
BERKELEY, CALIFORNIA 94720